foods

MDPI

Article

Optimization and Field Feasibility Evaluation of a Bent-Pipe Pneumatic Conveying Device for Bulk Tea Fresh Leaves Based on CFD-DEM

Luofa Wu [1,*], Jin Xiong [1], Shifu Shu [1], Chunwang Dong [2] and Hao Fu [3]

[1] Institute of Agricultural Engineering, Jiangxi Academy of Agricultural Sciences, Nanchang 330200, China
[2] Tea Research Institute of the Chinese Academy of Agricultural Sciences, Hangzhou 310013, China
[3] Shanyi Intelligent Equipment Co., Ltd., Yingtan 335200, China
* Correspondence: wlfjx001@163.com; Tel.: +86-138-7919-8039

Abstract

Thin flake-like fresh tea leaves tend to deposit and block the bend pipe during pneumatic conveying in self-propelled bulk-tea harvesters, and existing work gives little direct support for rapid parameter determination of such equipment. A CFD–DEM gas–solid coupling model was therefore built, in which non-spherical ball-cluster particles were reconstructed from 3D-scanned leaves, and the critical blockage-risk zones in the bend pipe were identified. Taking the air velocity at the fan outlet, the pipe inlet angle, and the side length of the feeding inlet as experimental factors, and the blockage rate as an evaluation indicator, 45 coupled simulations covering the spring, summer, and autumn seasons were conducted following a Box–Behnken design. Quadratic polynomial regression models were then established to describe response trends and support parameter screening. The results showed that the regression models for the three seasons were significant ($p < 0.05$), with R^2 values above 0.92, and were used to describe conditional average trends within the investigated design space. For summer and autumn fresh tea leaves, the predicted average blockage rate decreased with increasing fan outlet air velocity and pipe inlet angle. For all three seasons, the predicted average blockage rate first decreased and then increased as the feed inlet side length increased. Considering the high-desirability parameter regions and prototype manufacturing requirements, a practical parameter combination was selected, comprising a fan outlet air velocity of 25–30 m/s, a pipe inlet angle of 20°, and a feed inlet side length of 0.135 m. Field feasibility evaluation tests conducted at a fan outlet air velocity of 30 m/s, a pipe inlet angle of 20°, and a feed inlet side length of 0.135 m yielded blockage rates of 0.00% for spring and autumn fresh tea leaves and 0.61% for summer fresh tea leaves, demonstrating stable conveying under the tested field conditions. These findings provide a reference for parameter selection and the engineering design of pneumatic conveying equipment for fresh tea leaves used in bulk tea production.

Keywords: bulk tea; fresh tea leaves; pneumatic conveying; parameter optimization; CFD-DEM coupling

Check for updates

Academic Editor: Ramagopal Uppaluri

Received: 18 September 2026
Revised: 21 November 2026
Accepted: 23 November 2026
Published: 26 November 2026

Copyright: © 2026 by the authors. Licensee MDPI, Basel, Switzerland. This article is an open access article distributed under the terms and conditions of the Creative Commons Attribution (CC BY) license.

1. Introduction

Tea ranks among the most widely consumed non-alcoholic beverages worldwide. According to the 2025 statistical bulletin of the International Tea Committee, global production of made tea reached 7.2664 million tons in 2025 [1], of which China contributed 3.92 million tons, accounting for 53.9% of the total. In contrast, the mechanized harvesting rate of

Chinese tea gardens was only 41.43% in 2023 [2], far below the national average of 68.02% for all crops [3]. This gap mainly arises because tea gardens are mostly located in hilly and mountainous areas, where low standardization and poor machine-accessibility hinder large-scale mechanized harvesting. The mechanized harvesting equipment for bulk tea mainly includes single-/double-person tea plucking machines, ride-on tea plucking machines, and self-propelled tea harvesters [4,5]. In hilly tea gardens, large height differences between tea rows and low field standardization are common [6]. Single- and double-person plucking machines rely entirely on manual pushing, which involves high labor intensity, large workforce demand, and poor operational safety. Ride-on tea plucking machines are expensive, weak in climbing ability, and restricted to fixed row spacing, so their application scenarios are severely limited. By contrast, self-propelled tea harvesters have a compact structure, good trafficability, and low labor and workload requirements, making them the preferred machine type for tea gardens in hilly and mountainous regions.

Leaf collection and conveying are key stages of tea harvesting operations, mainly divided into mechanical conveying and pneumatic conveying. Mechanical conveying, which includes bucket-elevating and belt conveying, causes little leaf damage and consumes less energy, but requires a large installation area and high investment; it suits the integrated conveying equipment used for famous and high-quality tea [7,8]. Pneumatic conveying can be divided into positive-pressure blowing and negative-pressure suction types; it occupies little space, requires modest investment, and delivers high efficiency, but consumes more power, making it well suited for use on individual harvesting machines. Among these, the negative-pressure suction type is mostly applied to premium-tea picking robots [9], whereas the positive-pressure blowing type is structurally compatible with leaf collection in bulk tea harvesters [10], although practical applications of pneumatic leaf conveying in such machines remain scarce. Studies on the pneumatic conveying of fresh tea leaves fall into three categories: airflow-field analysis, tea-particle modelling, and gas–solid coupled simulation. For the pneumatic conveying process of fresh tea leaves, some scholars used the CFD numerical simulation method to analyze the airflow distribution of the leaf-collecting chamber and guide baffles of tea harvesters; however, such studies focused only on the characteristics of the gas-phase flow field and could not characterize the actual motion of fresh leaves in the airflow [11]. However, refined optimization was not carried out, and no multiple regression model was established for quantitative parameter analysis. Some scholars investigated the effects of structural parameters of the leaf-collecting pipeline, such as the taper of the main pipe, the number of branch pipes, and the outlet diameter of branch pipes, based on the CFD method, which effectively improved the airflow uniformity at the pipeline outlet; however, gas–solid coupling analysis with tea leaf material was not performed [12]. Some studies on negative-pressure leaf collection can achieve fresh leaf collection, but the experimental devices have no long-distance conveying pipeline with multiple bends, which differs from the actual conveying conditions of tea harvesters in the field [13,14]. Other researchers completed the particle modeling of fresh leaves using the multi-sphere method and conducted a CFD-DEM coupling simulation of the gas–solid two-phase flow in the leaf-collecting pipeline of a ride-on tea plucking machine [15], clarifying the mechanism by which the bend and feeding inlet induce leaf deposition. To simplify the simulation model, some studies treated dried tea material as spherical particles [16] and investigated the effects of different airflow velocities and particle weights on the winnowing performance of dried tea; however, fresh leaves are flexible flaky materials, and the spherical-particle simplification cannot match the actual conveying conditions. Other scholars took finished dried tea as the research object and proposed a weight-to-frontal-area ratio index to quantify differences in the aerodynamic properties of tea, clarifying the divergence mechanism of the drift trajectories between tea leaves and tea stems [17]; however, the research object

was finished dried tea, which cannot be directly adapted to the pneumatic conveying of flexible fresh leaves in the field. In addition, many scholars have studied the winnowing mechanism and simulation modeling of tea. Some scholars constructed a numerical method for the two-phase flow of flexible flaky materials based on the immersed boundary–lattice Boltzmann method (IB-LBM) [18], revealing the horizontal airflow sorting mechanism of machine-plucked fresh leaves; the experimental results showed that this method performed well for sorting small leaf materials but had poor adaptability to one-bud–one-leaf, one-bud–two-leaf, and multi-leaf materials. Some scholars used the CFD-DEM coupling simulation method to investigate the gas–solid two-phase motion in a green-tea winnowing chamber, simulating fresh and dried tea particles with multi-sphere discrete element particles and verifying the feasibility of the coupling simulation method in predicting the airflow drift and grading distribution of tea [19]. In addition, the CFD-DEM coupling simulation method has been widely applied to the pneumatic conveying of agricultural materials; beyond tea sorting, it has been used for the structural optimization and mechanism analysis of maize air-suction seed-metering devices [20], pneumatic conveying devices of cotton pickers [21], and conveying devices for dried safflower filaments [22], demonstrating considerable reliability. In summary, three limitations remain in both research and engineering application. First, pneumatic conveying simulations of agricultural materials mostly assume spherical or near-spherical particles; modelling and parameter optimization tailored to thin, flake-like fresh tea leaves are still insufficiently connected, so the results can hardly serve as a direct basis for pipe structural design. Second, published work on tea-leaf conveying focuses on flow-field characterization and lacks parameter optimization methods oriented to equipment development, which slows down engineering parameter determination. Third, seasonal differences in the physical properties of spring, summer, and autumn leaves have rarely been considered systematically, leaving the seasonal adaptability of the optimized parameters unclear for year-round harvesting operations.

Guided by the practical need to solve leaf deposition and blockage in the conveying bend of self-propelled bulk-tea harvesters, this study applied CFD–DEM gas–solid coupled simulation. Non-spherical fresh-leaf particles were constructed from 3D-scanned geometry through multi-sphere clustering. Fan outlet wind speed, pipe inlet angle, and feed-inlet side length were selected as the key structural and operating parameters, with blockage rate and fresh-leaf conveying rate as the core evaluation indices. Box–Behnken response surface experiments were conducted for the three seasonal leaf types; quantitative regression models were built to search the parameters and to verify the consistency of the structural parameters across seasons. A general engineering scheme of "fixed structural parameters plus adjustable wind speed" was then proposed. The scheme was finally verified through prototyping of a single unit and field experiments at two sites across three seasons, aiming to provide a practical reference for engineering design and parameter selection of bulk-tea pneumatic conveying equipment and to reduce prototyping iteration costs.

2. Materials and Methods

2.1. Physical Properties of Fresh Bulk Tea Leaves

The fresh bulk tea leaves used in the experiments were sampled from the Huangma Tea Base in Nanchang County. The tea cultivar was Fuding Dabai, which is suitable for mechanized harvesting, and the tea trees were over 40 years old. Sampling was carried out during the bulk tea harvesting periods of spring (18 April 2025), summer (16 July 2025), and autumn (4 September 2025), and 100 fresh tea leaves free of insect damage were randomly selected in each season for measurement [23,24]. The basic geometric dimensions of the leaves were measured with a vernier caliper (Figure 1a); the leaf density was measured by the water displacement method in five parallel tests. The leaf dimensions

and density were taken as the overall mean of the 100-leaf sample, while the average mass was determined separately for each leaf type; and tensile tests were performed on the leaves, which were cut into strip-shaped specimens, using a TMS-PRO texture analyzer (Figure 1b), with 15 parallel tests in total. The parameters of the fresh tea leaves used in the simulation are listed in Table 1. Preliminary measurements of the static angle of repose of fresh tea leaves were conducted using the cylinder-lifting method, with ten replicate tests. However, interlocking and bridging readily occurred among the fresh tea leaves, and the pile geometry was sensitive to the initial placement of the material, resulting in considerable variability among replicates. Consequently, a stable relationship for DEM parameter calibration could not be established. Therefore, the angle-of-repose measurements were not used for the inverse calibration of DEM contact parameters. The current parameter set was used only to develop a baseline DEM model for the pneumatic conveying of fresh tea leaves. The simulation results are intended primarily for comparing operating conditions and analyzing average trends under the same modeling assumptions and should not be interpreted as fully validated quantitative predictions of absolute outcomes.

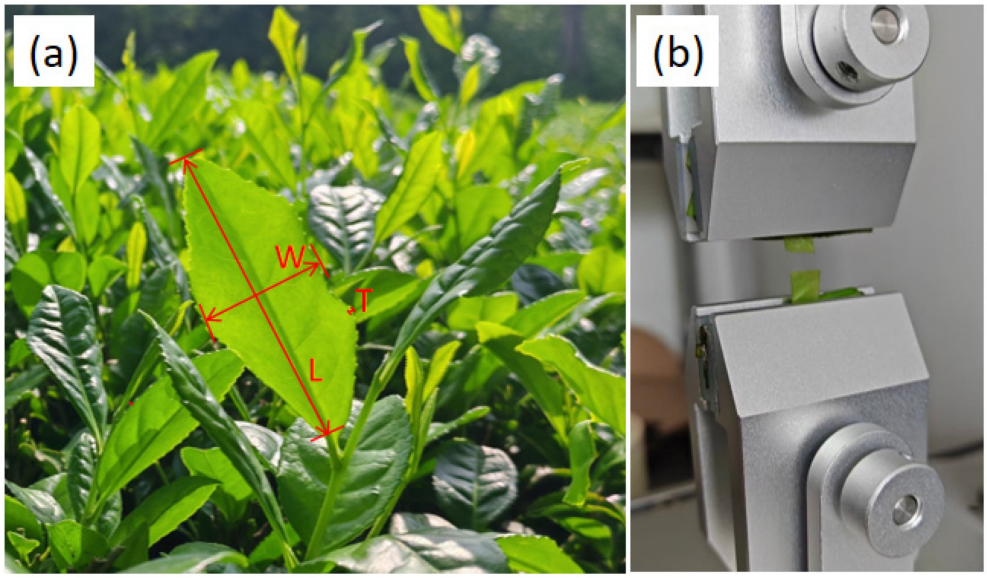


Figure 1. Measurement of physical parameters of fresh bulk tea leaves: (**a**) schematic diagram of leaf length, width, and thickness; (**b**) tensile test of a leaf.

Table 1. Physical properties of fresh tea leaves in different seasons.

Parameter	Symbol	Unit	Spring			Summer			Autumn		
			One-Leaf	Two-Leaf	Three-Leaf	One-Leaf	Two-Leaf	Three-Leaf	One-Leaf	Two-Leaf	Three-Leaf
Average leaf length	$\bar{l}$	mm		66.1			44.2			42.1	
Average leaf width	$\overline{w}$	mm		28.5			17.5			16.6	
Average leaf thickness	$\bar{t}$	mm		0.8			0.61			0.59	
Average mass	$\overline{m}$	g	0.25	0.49	0.79	0.14	0.26	0.42	0.13	0.22	0.39
Average leaf density	$\bar{\rho}$	kg·m^{-3}		506.3			548.5			560.2	
Moisture content	ω	%	84.31	79.60	77.80	80.20	76.52	75.37	79.50	75.98	75.12
Mass fraction	w	%	43.19	16.89	39.92	24.08	19.04	56.88	26.12	21.34	52.54

Table 1. *Cont.*

Parameter	Symbol	Unit	Spring			Summer			Autumn		
			One-Leaf	Two-Leaf	Three-Leaf	One-Leaf	Two-Leaf	Three-Leaf	One-Leaf	Two-Leaf	Three-Leaf
Elastic modulus	E	MPa		4.9			4.59			4.45	
Poisson's ratio	v	/		0.4			0.38			0.35	
Static friction coefficient (leaf–leaf)	μ_{s1}	/		0.95			0.92			0.91	
Kinetic friction coefficient (leaf–leaf)	μ_{k1}	/		0.75			0.74			0.73	
Static friction coefficient (leaf–aluminum)	μ_{s2}	/		0.65			0.63			0.62	
Kinetic friction coefficient (leaf–aluminum)	μ_{k2}	/		0.53			0.52			0.51	
Restitution coefficient	e	/		0.23			0.28			0.25	

Fresh tea leaves are flat, non-spherical particles; if the spherical particle assumption is adopted directly, the drag force calculation and the rotational characteristics of the particles will be significantly distorted. Therefore, in this study, a HOLON B71 handheld 3D scanner was used to collect the point cloud data of fresh leaves (Figure 2a). After preprocessing and optimization, the 3D geometric model was reconstructed, and particle filling was then performed on the geometric model to generate clustered-sphere particles that conform to the actual shape of the fresh leaves (Figure 2b) [25,26]. This modeling method can reproduce the flat shape and moment of inertia of fresh tea leaves, while retaining the computational efficiency of the spherical-particle contact model.

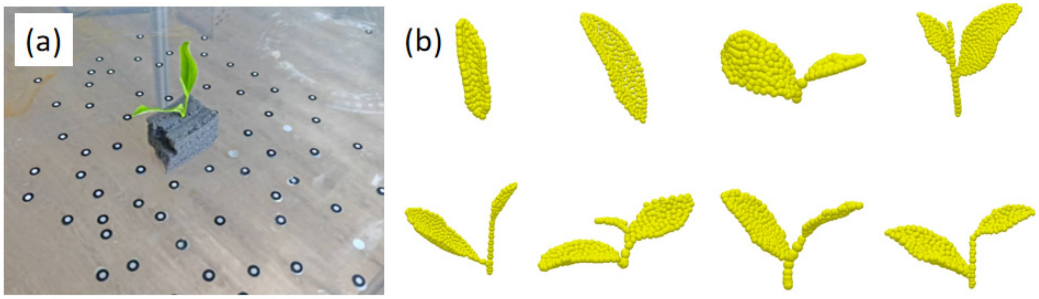


Figure 2. Discrete element model of bulk tea leaf particles: (**a**) acquisition of point cloud data of fresh bulk tea leaves using a 3D scanner; (**b**) particle model.

2.2. Overview of the Self-Propelled Bulk Tea Harvester and Its Leaf-Conveying Components

The self-propelled bulk tea harvester used for the harvesting operation in this study (Figure 3; manufactured by Jiangxi Shanyi Intelligent Equipment Co., Ltd., Nanchang, China) mainly consists of a crawler chassis, a tea-cutting header device, a lifting mechanism, a pneumatic conveying device, and an intelligent control system. Its main parameters are listed in Table 2. To meet the requirement of traveling between tea rows, the whole machine adopts a compact structural design, with a chassis width of 60 cm and an overall length of

220 cm. Before harvesting, the tea-cutting device is adjusted to a suitable height. During operation, the machine moves forward along the tea ridge at a constant speed; the fresh tea leaves are cut off by the cutter and fall onto the cutter baffle, then are blown by the airflow of the leaf-collecting air duct to the screw auger, conveyed by the auger to the feeding inlet of the pneumatic conveying device, and finally collected into the leaf collection bag through the pneumatic conveying device.

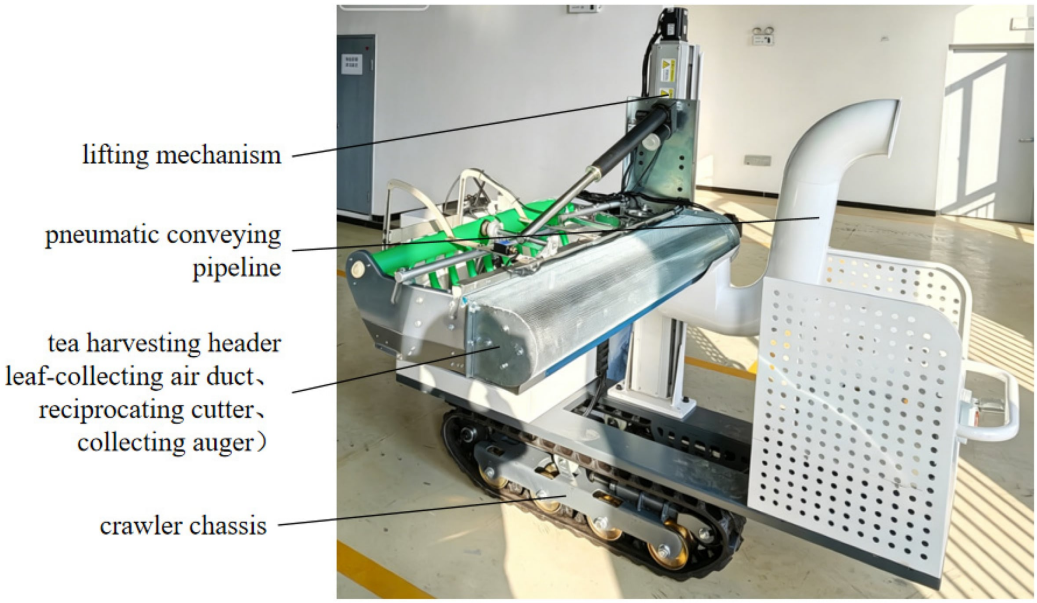


Figure 3. Overall view of the self-propelled bulk tea harvester.

Table 2. Main technical parameters of the self-propelled bulk tea harvester.

Item	Value
Mass of the harvester/kg	420
Overall dimensions (length × width × height)/m	2.20 × 1.60 × 1.81
Maximum traveling speed/(m·s^{-1})	0.9
Lifting height of the header/m	0.4~1.2
Working width of the header/m	1.0

The pneumatic conveying device consists of a fan, connecting hoses, a pneumatic conveying pipeline, and a leaf-collecting air duct. Its working principle is shown in Figure 4a: the rotation of the fan generates a positive-pressure airflow (the black arrows indicate the airflow direction), which is delivered through the connecting hoses into the pneumatic conveying bend pipe and the leaf-collecting air duct, respectively. A negative pressure is formed at the feeding inlet of the pneumatic conveying pipeline, which drives the fresh tea leaves into the pipeline (the green arrows indicate the moving direction of the leaves); the leaves are then conveyed along the pipeline with the airflow and finally enter the leaf collection bag through the outlet, completing the collection of machine-harvested fresh tea leaves. As shown in Figure 4b, the pneumatic conveying bend pipe adopts a combination of two 90° bends and a vertical pipe section; the pipe has a circular cross-section with an inner diameter of 160 mm, and the vertical section is 300 mm in length.

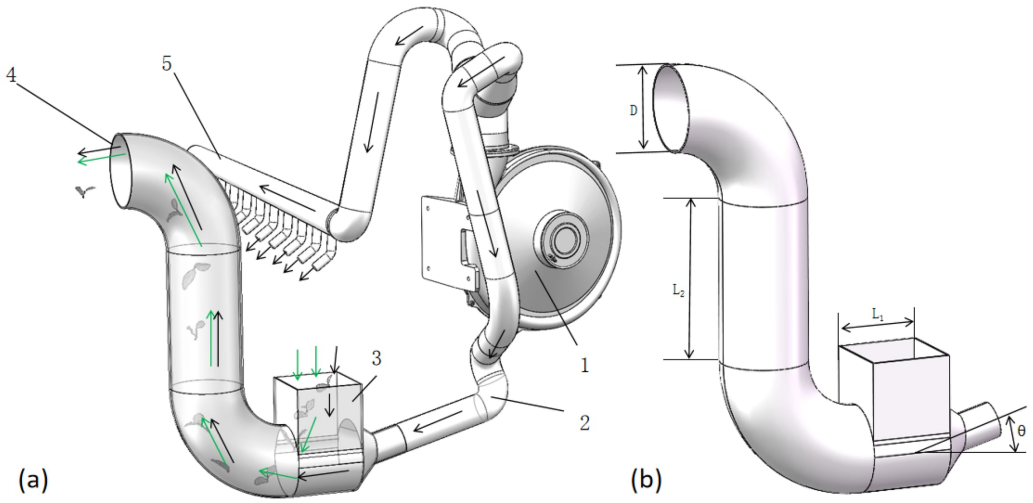


Figure 4. Working principle and structure of the pneumatic conveying pipeline: (**a**) working principle diagram. 1. Fan; 2. connecting hose; 3. feeding inlet of the pneumatic conveying pipeline; 4. outlet of the conveying pipeline; 5. leaf-collecting air duct; (**b**) structural diagram of the pneumatic conveying pipeline.

2.3. Motion Analysis of Fresh Tea Leaves in the Pneumatic Conveying Pipeline

2.3.1. Governing Equations of the Fluid Phase

During the conveying process, the fluid (air) generated by the fan serves as the carrier for the motion of fresh tea leaves and plays a dominant role in their movement. Assuming that the fluid is incompressible, the lattice Boltzmann method (LBM) was employed to solve the fluid motion [18,27,28], in which the macroscopic flow field characteristics are represented by the evolution of the discrete particle distribution function. The evolution equation is given in Equation (1):

$$f_i(x + e_i\Delta t + \Delta t) - f_i(x,t) = \Omega_i(f(x,t)) \quad (1)$$

where f_i is the particle distribution function in the i-th direction; e_i is the discrete velocity vector; Δt is the time step; and Ω_i is the collision operator.

The Bhatnagar–Gross–Krook (BGK) approximation was adopted to simplify the collision operator, yielding:

$$\Omega_i = -\frac{1}{\tau}(f_i - f_i^{eq}) \quad (2)$$

where τ is the dimensionless relaxation time and f_i^{eq} is the equilibrium distribution function.

The macroscopic density ρ and velocity u of the fluid are obtained from the moments of the particle distribution functions:

$$\rho = \sum_i f_i, \rho u = \sum_i f_i e_i \quad (3)$$

LBM is inherently suited to complex boundaries and transient turbulence computation, and can accurately capture the vortex structures and velocity gradients inside the pipeline. In this study, the large eddy simulation (LES) method was employed for the numerical computation [29], and the wall-adapting local eddy-viscosity (WALE) model was selected as the subgrid-scale stress model. The WALE model can correctly describe the decay of eddy viscosity in the near-wall region without near-wall damping functions, and its computational expression is as follows:

$$v_t = \frac{(G^{\mathrm{d}}_{\alpha\beta}G^{d}_{\alpha\beta})^{\frac{3}{2}}}{(S_{\alpha\beta}S_{\alpha\beta})^{\frac{5}{2}} + (G^{d}_{\alpha\beta})^{\frac{5}{4}}}\Delta_f^2 \quad (4)$$

where

$$S_{\alpha\beta} = \frac{g_{\alpha\beta} + g_{\beta\alpha}}{2} \tag{5}$$

$$G^{\mathrm{d}}_{\alpha\beta} = \frac{1}{2}(g^2_{\alpha\beta} + g^2_{\beta\alpha}) - \frac{1}{3}\delta_{\alpha\beta}g^2_{\gamma\gamma} \tag{6}$$

$$\Delta_f = C_w \Delta x \tag{7}$$

where v_t is the subgrid-scale eddy viscosity; $G^d{}_{\alpha\beta}$ and $S_{\alpha\beta}$ are the resolved-scale tensor and the strain-rate tensor, respectively; $\delta_{\alpha\beta}$ is the Kronecker delta; Δf is the filter width; C_w is a constant (taken as 0.325); Δx is the unit grid scale; and $g_{\alpha\beta}$, $g_{\beta\alpha}$, and $g_{\gamma\gamma}$ are the strain-rate tensors, which can be obtained as second-order moments by the LBM. The subscripts α, β, and γ denote the spatial directions, taking values of 1 and 2 in two-dimensional cases and 1, 2, and 3 in three-dimensional cases.

2.3.2. Governing Equations of the Particle Phase

The fresh tea leaves were treated as discrete particles, and the discrete element method (DEM) was employed to simulate their motion behavior in the fluid, with emphasis on tracking the translation and rotation of the particles. The motion of the particles follows Newton's second law:

$$m_p \frac{dv_p}{dt} = F_f + F_c + m_p g \tag{8}$$

$$I_P \frac{dw_p}{dt} = T_c \tag{9}$$

where m_p is the particle mass; v_p is the translational velocity of the particle; I_p is the moment of inertia of the particle; ω_p is the angular velocity of the particle; Ff is the force exerted by the fluid on the particle; F_c is the contact force between particles and walls; g is the gravitational acceleration; and T_c is the contact torque.

The force exerted by the fluid on the particle is dominated by the drag force, while the lift force, pressure gradient force, and virtual mass force are also taken into account. Given the non-spherical shape of fresh tea leaves, the Ganser drag model was adopted to calculate the drag force [30]; this model introduces a sphericity correction term, making it suitable for the drag characteristics of flat particles:

$$F_f = \frac{1}{2} C_d \rho_f A_p \left| u_f - v_p \right| (u_f - v_p) \tag{10}$$

$$C_d = \frac{24}{\mathrm{Re}_p K_1 K_2}\left[1 + 0.1118(\mathrm{Re}_p K_1 K_2)^{0.6567}\right] + \frac{0.4305}{1 + 3305/(\mathrm{Re}_p K_1 K_2)} \tag{11}$$

where C_d is the drag coefficient; ρ_f is the fluid density; A_p is the frontal area of the particle; u_f is the local fluid velocity; Re_p is the particle Reynolds number; and K_1 and K_2 are the non-spherical correction factors, which are directly related to the particle sphericity ψ.

The contact forces were calculated using the Hertz–Mindlin no-slip contact model, and the normal contact force F_n and tangential contact force F_t are given by:

$$F_n = \frac{4}{3} E^* \sqrt{R^*} \delta_n^{\frac{3}{2}} \tag{12}$$

$$F_t = -8G^* \sqrt{R^* \delta_n} \delta_t \tag{13}$$

where E^* is the equivalent elastic modulus; R^* is the equivalent particle radius; δ_n is the normal overlap; G^* is the equivalent shear modulus; and δ_t is the tangential overlap.

2.4. Coupled Simulation of Pneumatic Conveying for Machine-Harvested Fresh Tea Leaves

The pneumatic conveying of fresh tea leaves involves strongly coupled, nonlinear behavior, and the numerical simulation must account for both the drag interaction between the leaves and the fluid and the contact interactions among particles. Therefore, this study adopted a coupled computational fluid dynamics (CFD) and discrete element method (DEM) approach: the continuous-phase flow field was solved by the lattice Boltzmann method, the discrete-phase tea leaf particles were tracked by the discrete element method, and one-way coupling from the flow field to the particles was realized through the drag force, thereby reproducing the dynamic behavior of fresh tea leaves in the airflow [31]. The airflow velocities in the flow field investigated in this study were mainly within the range of 15–30 m/s. Taking the case with a pipe inlet angle of 20°, a feed inlet side length of 0.135 m, and a fan outlet air velocity of 30 m/s (A20_L0.135_V30) as an example, the outlet air mass flow rate was 0.170 kg/s, and the simulated feed rate was 0.007 kg/s. The corresponding solids-to-air mass ratio was approximately 0.041 kg/kg, and the nominal particle volume fraction was estimated to be approximately 0.009%. Therefore, under this feed condition, the overall particle phase was relatively dilute, and one-way coupling was adopted as a numerical simplification. The applicability of this simplification does not extend directly to higher field feeding rates or localized blockage conditions. Because the fresh tea leaves were represented by multi-sphere non-spherical particles, a higher feeding rate would substantially increase the number of particles and the computational cost of contact calculations. To complete the 45 coupled simulations across the three seasons, the simulated feed rate was set to 7 g/s to reduce the computational cost rather than to represent the actual field feeding rate of the tea harvester. This setting ensured that all 45 simulations used the same particle-generation duration, total feed mass, and statistical window, thereby enabling the effects of fan outlet air velocity, pipe inlet angle, and feed inlet side length on short-term leaf conveying and retention behavior within the pipe to be compared under identical numerical boundary conditions. Accordingly, the simulation results were primarily used for comparing operating conditions and screening parameters under the same reference conditions, rather than for directly predicting the field throughput of the complete machine or absolute blockage rates under continuous operation.

The boundary conditions for the fluid phase were set as follows: the fan outlet section was defined as a velocity inlet, with the air velocity set to the design value V and a turbulence intensity of 5%; the tea leaf feeding inlet was defined as a pressure inlet with a relative pressure of 0 Pa; the pipeline outlet and the remaining openings were defined as pressure outlets with a relative pressure of 0 Pa; and the pipeline walls were set as no-slip adiabatic walls. The flow field was solved in steady-state mode with adaptive mesh refinement enabled, and the converged flow field was then used as the background flow field for particle motion. The particle motion was solved in Altair EDEM using one-way coupling. Three particle factories were placed at the feed inlet to generate one-leaf, two-leaf, and three-leaf particles from the scanned and reconstructed models; the particle positions, orientations, and release times were all randomly initialized. For the numerical reference condition, the total particle mass flow rate was set to 7 g/s, and the proportions of the three leaf types were adjusted by season (Table 3). The particles were generated continuously from 0 to 2 s, and the entire simulation was computed up to 3 s. The pipeline walls were defined as collision boundaries with normal and tangential contact parameters specified, and the outlet was defined as a particle escape boundary.

Table 3. Mass flow rate settings of different leaf types at the particle factories in different seasons.

Leaf Type	Spring		Summer		Autumn	
	Mass Flow Rate/(g·s^{-1})	Total Mass in 2 s/(g)	Mass Flow Rate/(g·s^{-1})	Total Mass in 2 s/(g)	Mass Flow Rate/(g·s^{-1})	Total Mass in 2 s/(g)
One-leaf	3.023	6.046	1.686	3.372	1.828	3.656
Two-leaf	1.182	2.364	1.333	2.666	1.494	2.988
Three-leaf	2.794	5.588	3.982	7.964	3.678	7.356
Total	7	14	7	14	7	14

To assess mesh sensitivity, transient LBM–LESs were conducted using coarse, medium, and fine meshes with lattice sizes of 15, 10, and 6.7 mm, respectively, at a pipe inlet angle of 20°, a feed inlet side length of 0.135 m, and a fan outlet air velocity of 30 m/s. All other settings, including the boundary conditions, subgrid-scale model, and adaptive mesh-refinement strategy, were kept identical. Outlet mass-flow time series were integrated using the trapezoidal rule and divided by their respective time-window lengths to obtain time-averaged values. Air velocity was monitored at the same outlet location for all three meshes, and relative deviations were calculated using the medium mesh as the reference. The results are presented in Table 4.

Table 4. Results of the mesh sensitivity analysis.

Mesh Scheme	Lattice Size (mm)	Time-Averaged Outlet Air Mass Flow Rate (kg/s)	Mean Air Velocity at the Fixed Outlet Monitoring Point (m/s)	Deviation from the Medium Mesh (Mass Flow Rate/Velocity)
Coarse	15	0.175	10.11	2.94%/4.80%
Medium	10	0.170	10.62	/
Fine	6.7	0.159	10.13	6.47%/4.61%

The time-averaged outlet mass flow rates for the coarse, medium, and fine meshes were 0.175, 0.170, and 0.159 kg/s, respectively, and the corresponding monitoring-point velocities were 10.11, 10.62, and 10.13 m/s. Relative to the medium mesh, mass-flow deviations were 2.94% for the coarse mesh and 6.47% for the fine mesh, while velocity deviations were 4.80% and 4.61%, respectively. Since the monitoring-point velocity varied non-monotonically and the mass flow rate still differed by 6.47% between the medium and fine meshes, these results indicate mesh sensitivity rather than grid independence or asymptotic convergence. The medium mesh was used in subsequent simulations to improve computational efficiency. The simulation results were used only for comparisons among operating conditions, factor-effect analyses, and parameter screening under identical numerical settings.

The experimental design adopted the Box–Behnken design (BBD) of response surface methodology [32], and CFD-DEM coupled simulation experiments were conducted with spring, summer, and autumn bulk tea leaves as the conveying objects. The air velocity at the fan outlet (V), the pipe inlet angle (θ), and the side length of the feeding inlet (L) were selected as the experimental factors, each with three levels. The correspondence between the factor levels and their coded values is shown in Table 5. The feeding inlet has a square cross-section, and its side length directly determines the feeding area and the initial distribution state of the particles. The three center points involved independent numerical runs using different random seeds only, while all other model parameters and boundary conditions were kept identical. Pure error was estimated from the deviations of the three center-point observations from their mean, with two degrees of freedom, and was used in the lack-of-fit test. This pure error reflects only the variability in numerical simulation results arising from different random seeds and does not represent random errors caused by variations in field materials or environmental conditions. Identical experimental schemes

and boundary conditions were applied to the tea leaves of all three seasons, with only the physical and mechanical parameters of the DEM particle model replaced, yielding a total of 45 coupled simulation runs. The standard order, run order, and factor coding of the experimental scheme are shown in Table 6.

Table 5. Factors and levels of the response surface experiment with coded values.

Factor	Symbol	Unit	Coded Level		
			1	**0**	**−1**
Air velocity at fan outlet	V	m/s	20	25	30
Pipe inlet angle	θ	°	10	15	20
Side length of feeding inlet	L	m	0.120	0.135	0.150

Note: V denotes the air velocity at the fan outlet; θ denotes the pipe inlet angle; and L denotes the side length of the feeding inlet. In the regression models, $A = V$, $B = \theta$, and $C = L$. The corresponding feeding-inlet areas are 0.0225, 0.018225, and 0.0144 m^2, covering the adaptation range of the rated feeding capacity of the tea harvester.

Table 6. Box–Behnken simulation experiment scheme.

Std Order	Run Order	V	θ	L
13	1	0	0	0
14	2	0	0	0
10	3	0	−1	−1
1	4	1	1	0
4	5	−1	−1	0
2	6	−1	1	0
9	7	0	1	−1
5	8	1	0	−1
3	9	1	−1	0
12	10	0	−1	1
15	11	0	0	0
6	12	−1	0	−1
7	13	1	0	1
8	14	−1	0	1
11	15	0	1	1

Two core response indicators, the blockage rate and the fresh-leaf conveying rate, were selected to comprehensively characterize the stability, conveying efficiency, and overall performance of the conveying system.

(1) Blockage rate: this indicator characterizes the blockage risk during conveying and is defined as the percentage of the mass of particles deposited inside the pipeline to the total feeding mass, calculated as:

$$P_{\text{block}} = \frac{m_{retention}}{m_{total}} \times 100\% \tag{14}$$

where P_{block} is the blockage rate, in %; $m_{retention}$ is the total mass of particles remaining within the designated pipe monitoring region at the end of the specified statistical time window of 3 s, with these particles classified as retained particles, in g; and m_{total} is the total feeding mass over the same period, which is 14 g in the simulation.

(2) Fresh-leaf conveying rate (mass of tea leaves conveyed per second): This indicator characterizes the conveying efficiency of the system and is defined as the mass of fresh tea leaves delivered to the pipeline outlet per unit time, reflecting the actual conveying capacity of the system, calculated as:

$$q_m = \frac{m_{out}}{\Delta t} \tag{15}$$

where q_m is the fresh-leaf conveying rate, in g/s; m_{out} is the total mass of fresh leaves collected at the outlet within the time interval Δt, in g; and Δt is the statistical time step, in s.

Since the total feed mass and the counting window were identical for all runs, the two indices satisfy $q_m = (14/3) \times (1 - P_{block}/100)$, i.e., they are two algebraic expressions of the same mass balance rather than independent responses, conveying complementary engineering meanings (blockage risk versus actual throughput).

Regression analysis and significance testing were performed on the experimental results, and second-order polynomial regression models were established between each response indicator and the experimental factors, in the following form:

$$Y = b_0 + \sum_{i=1}^{3} b_i X_i + \sum_{i=1}^{3} b_{ii} X_i^2 + \sum_{i<j=2}^{3} b_{ij} X_i X_j \quad (16)$$

where Y is the predicted value of the response indicator; b_0 is the constant term; b_i is the coefficient of the linear term; b_{ii} is the coefficient of the quadratic term; b_{ij} is the coefficient of the interaction term; and X_i and X_j are the coded values of the factors.

3. Results

3.1. Motion Behavior of Fresh Tea Leaves During Bend-Pipe Conveying

Taking the conveying condition with a pipe inlet angle of 20°, a feeding-inlet side length of 0.135 m, and a fan outlet air velocity of 25 m/s as an example, the central symmetric section of the pipeline, the bend section, and the outlet cross-section were selected to examine the pneumatic conveying process in terms of velocity distribution and pressure characteristics, thereby revealing the underlying mechanisms of particle transport and deposition.

The velocity contour of the flow field (Figure 5a) reveals three flow characteristics.

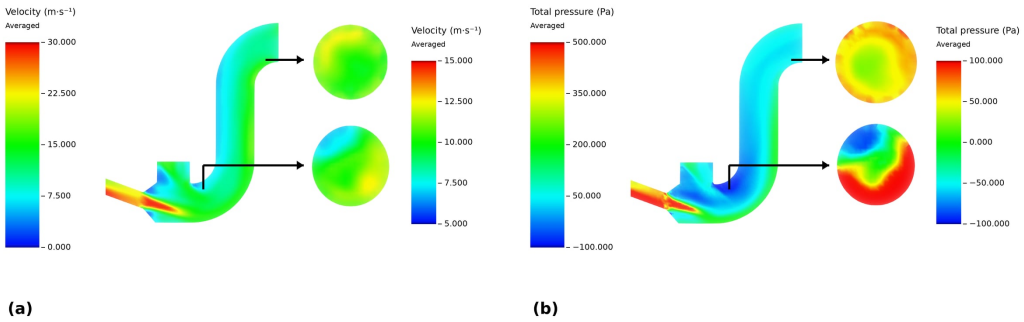


Figure 5. Velocity and pressure contours of the flow field at a pipe inlet angle of 20° and a feeding-inlet side length of 0.135 m: (**a**) velocity contour; (**b**) pressure contour.

Near the pipe inlet, a distinct low-velocity triangular recirculation zone formed at the lower wall. The high-speed jet diffused along the mainstream direction after entering, but a local recirculation structure developed close to the lower wall, where the airflow drag weakened markedly and could no longer entrain the thin flake leaves effectively; the particles therefore settled readily, making this zone the key inducement of initial leaf accumulation. Increasing the inlet angle effectively suppressed the recirculation, widened the high-velocity coverage, and improved the initial acceleration of the particles.

In the bend section, centrifugal inertia dominated the flow and produced a pronounced velocity stratification. The velocity at the outer wall was markedly higher than that at the inner wall, creating a strong transverse velocity gradient; driven by inertia, the fresh-leaf particles drifted toward the outer wall, whereas the inner wall remained in a low-velocity

state for long periods where particle followability was poor, leaving a risk of retention and accumulation.

The velocity distribution at the outlet section was generally uniform, decreasing slightly from the upper to the lower part. The difference between the maximum and minimum velocities was about 3 m/s, the gradient was gentle, and no distinct low-velocity stagnation zone appeared, meeting the uniformity requirement for pneumatic conveying.

The pressure contour of the flow field (Figure 5b) reveals three pressure characteristics:

The local negative-pressure environment in the feeding-inlet region guides the particles steadily into the pipeline.

The pressure gradient between the outer and inner sides of the bend is the core mechanism inducing recirculation vortices and particle blockage. Under centrifugal deflection, the outer side of the bend exhibits high pressure while the inner side exhibits low pressure; the resulting transverse pressure difference drives the airflow back toward the inner side, forming a recirculation vortex. This vortex structure prolongs the residence time of particles and induces the entanglement and agglomeration of leaves, constituting the main source of blockage risk in the pipeline.

In addition, air velocity regulates conveying stability in a non-monotonic, bidirectional manner. A moderate increase in air velocity enhances the aerodynamic drag, improves particle suspension and acceleration, and suppresses the formation of low-velocity dead zones; however, an excessively high velocity amplifies the centrifugal pressure difference in the bend, intensifies the recirculation vortex there, and disturbs the particle trajectories, eventually leading to accumulation in the bend region.

To obtain an independent experimental reference for the gas-phase velocity at the outlet, local air velocities across the pipe outlet cross-section were measured under no-load conditions with a fan outlet air velocity of 25 m/s, a pipe inlet angle of 20°, and a feed inlet side length of 0.135 m. Measurements were performed using a handheld anemometer (DL333214, Deli; measurement range: 0–30 m/s; manufacturer-specified accuracy: $\pm 3\% \pm 0.1$ m/s). Three measurement points were positioned along the vertical centerline of the outlet cross-section, at one-quarter, one-half, and three-quarters of the cross-sectional height measured downward from the top of the outlet. The probe was held at each measurement point for 10 s before readings were taken. Five replicate measurements were performed at each point and averaged. The mean air velocities at the upper, middle, and lower measurement points were 12.3, 10.1, and 9.1 m/s, respectively, indicating a vertical distribution with higher velocities in the upper region and lower velocities in the lower region. This trend was qualitatively consistent with the simulated velocity distribution at the outlet cross-section shown in Figure 5a. These results provide an experimental reference for the gas-phase velocity at the outlet. However, they represent only local air velocities at three measurement points across the outlet cross-section and do not constitute comprehensive validation of the internal flow field within the pipe bends.

Taking autumn tea leaves as an example, the influence mechanisms of the pipeline structure and air velocity on particle conveying were further revealed by examining the conveying characteristics under different working conditions (Figure 6). The results show three findings.

An excessively small inlet angle is the dominant factor inducing particle accumulation at the first bend and subsequent pipeline blockage. A too-small inlet angle considerably widens the low-velocity stagnation zone in the feeding section, where the aerodynamic drag is insufficient to maintain the suspension velocity required for particles to pass through the bend; the particles then remain and accumulate at the first bend, gradually occupying the effective space of the pipeline and blocking the passage of subsequent particles, which eventually develops into blockage.

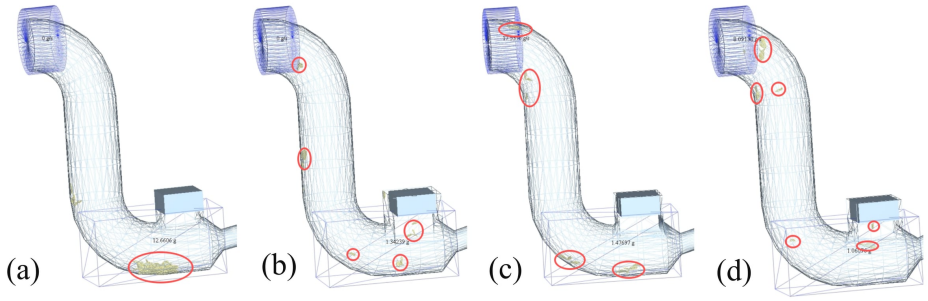


Figure 6. Positions of autumn fresh tea leaf particles under different structural parameters and air velocities: (**a**) A10L0.12V25, t = 2.56 s; (**b**) A15L0.15V30, t = 1.36 s; (**c**) A15L0.135V25, t = 1.8 s; (**d**) A20L0.135V30, t = 0.39 s. Note: A denotes the pipe inlet angle, L the feeding-inlet side length, V the fan outlet air velocity, and t the current time instant.Note:The red ellipse represents the position of the tea leaves.

The trajectories of particles in the bends are dominated by centrifugal effects and agree well with the velocity and pressure distributions of the flow field. The particles first move along the inner wall of the first bend; after transitioning through the vertical section, they turn toward the outer wall under the centrifugal force at the second bend. This motion pattern is consistent with the flow-field contour characteristics, verifying the reliability of the foregoing mechanism analysis.

The improvement of conveying performance by air velocity exhibits a significant marginal effect, and excessively high or low velocities both weaken the system stability. An appropriate increase in air velocity can enlarge the effective suspension zone in the middle of the pipeline and improve the overall suspension state of the particles; however, an excessively high velocity intensifies the airflow disturbance and local vortex strength inside the pipe, which in turn interferes with the stable transport of particles.

3.2. Effects of Conveying Parameters and Regression Modelling

3.2.1. Establishment and Significance Testing of the Regression Models

The coupled simulation results of pneumatic conveying for tea leaves of the three seasons are shown in Table 7.

Table 7. Coupled simulation results of pneumatic conveying for spring, summer, and autumn fresh tea leaves.

Std Order	Run Order	Season	Conveying Rate/(g·s^{-1})	Retained Mass per 14 g Leaves/(g)	Blockage Rate/(%)
13	1	Spring	3.1803	4.46	31.85
		Summer	2.7558	5.73	40.95
		Autumn	4.6667	0.00	0.00
14	2	Spring	4.6667	0.00	0.00
		Summer	2.4733	6.58	47.00
		Autumn	3.6820	2.95	21.10
10	3	Spring	4.4033	0.79	5.64
		Summer	4.6667	0.00	0.00
		Autumn	4.4033	0.79	5.64
1	4	Spring	1.3200	10.04	71.71
		Summer	1.2500	10.25	73.21
		Autumn	1.9433	8.17	58.36
4	5	Spring	4.6233	0.13	0.93
		Summer	4.5767	0.27	1.93
		Autumn	4.6233	0.13	0.93

Table 7. *Cont.*

Std Order	Run Order	Season	Conveying Rate/(g·s^{-1})	Retained Mass per 14 g Leaves/(g)	Blockage Rate/(%)
2	6	Spring	3.1933	4.42	31.57
		Summer	2.3433	6.97	49.79
		Autumn	3.9167	2.25	16.07
9	7	Spring	0.5033	12.49	89.21
		Summer	0.6900	11.93	85.21
		Autumn	0.0000	14.00	100.00
5	8	Spring	0.5033	12.49	89.21
		Summer	0.7267	11.82	84.43
		Autumn	1.1767	10.47	74.79
3	9	Spring	4.6667	0.00	0.00
		Summer	4.5733	0.28	2.00
		Autumn	4.6233	0.13	0.93
12	10	Spring	4.0800	1.76	12.57
		Summer	4.4833	0.55	3.93
		Autumn	4.3933	0.82	5.86
15	11	Spring	4.6233	0.13	0.93
		Summer	1.6732	8.98	64.15
		Autumn	4.4831	0.55	3.93
6	12	Spring	1.3967	9.81	70.07
		Summer	2.3750	6.87	49.11
		Autumn	2.0700	7.79	55.64
7	13	Spring	2.2467	7.26	51.86
		Summer	2.8867	5.34	38.14
		Autumn	1.8833	8.35	59.64
8	14	Spring	4.6667	0.00	0.00
		Summer	4.6667	0.00	0.00
		Autumn	4.6667	0.00	0.00
11	15	Spring	3.1900	4.43	31.64
		Summer	3.1100	4.67	33.36
		Autumn	3.6033	3.19	22.79

Based on the simulation results, a quadratic polynomial regression model was established for the blockage rate, fresh leaf conveying rate, fan outlet wind speed, pipe inlet angle, and feed inlet side length. The significance and fitting accuracy of the model were tested using analysis of variance (ANOVA), with a significance level of $\alpha = 0.05$. The summary of the model fitting accuracy and significance results is shown in Table 8.

Table 8. Analysis of variance (ANOVA) for the regression models of blockage rate and conveying rate for the three fresh tea leaf types.

Source	Coefficients	Standard Error	Sum of Squares	DF	Mean Square	F-Value	*p*-Value
Spring blockage rate [a]							
Model			14,853.30	9	1650.37	6.95 *	0.0230
A	−13.78	5.45	1518.40	1	1518.40	6.40 ^{NS}	0.0526
B	−25.62	5.45	5253.12	1	5253.12	22.14 **	0.0053
C	−19.76	5.45	3123.32	1	3123.32	13.16 *	0.0151
AB	10.27	7.70	421.72	1	421.72	1.78 ^{NS}	0.24
AC	−8.18	7.70	267.56	1	267.56	1.13 ^{NS}	0.3369
BC	16.13	7.70	1040.06	1	1040.06	4.38 ^{NS}	0.0905

Table 8. *Cont.*

Source	Coefficients	Standard Error	Sum of Squares	DF	Mean Square	F-Value	*p*-Value
A^2	16.57	8.02	1014.10	1	1014.10	4.27 ^{NS}	0.0936
B^2	−1.45	8.02	7.71	1	7.71	0.0325 ^{NS}	0.8640
C^2	25.29	8.02	2360.96	1	2360.96	9.95 *	0.0253
Residual			1186.52	5	237.30		
Lack of Fit			529.38	3	176.46	0.5371 ^{NS}	0.7020
Total			16,039.82	14			
conveying rate [b]							
Model			32.35	9	3.59	6.95 *	0.0230
A	0.6429	0.2542	3.31	1	3.31	6.40 ^{NS}	0.0526
B	1.20	0.2542	11.44	1	11.44	22.14 **	0.0053
C	0.9221	0.2542	6.80	1	6.80	13.16 *	0.0151
AB	−0.4792	0.3594	0.9184	1	0.9184	1.78 ^{NS}	0.24
AC	0.3817	0.3594	0.5827	1	0.5827	1.13 ^{NS}	0.3369
BC	−0.7525	0.3594	2.27	1	2.27	4.38 ^{NS}	0.0905
A^2	−0.7734	0.3741	2.21	1	2.21	4.27 ^{NS}	0.0936
B^2	0.0674	0.3741	0.0168	1	0.0168	0.0325 ^{NS}	0.8640
C^2	−1.18	0.3741	5.14	1	5.14	9.95 *	0.0253
Residual			2.58	5	0.5168		
Lack of Fit			1.15	3	0.3843	0.5371 ^{NS}	0.7020
Total			34.93	14			
Summer blockage rate [c]							
Model			12,440.88	9	1382.32	7.80 *	0.0179
A	−12.12	4.71	1174.91	1	1174.91	6.63 *	0.0497
B	−29.21	4.71	6827.55	1	6827.55	38.53 **	0.0016
C	−17.92	4.71	2567.58	1	2567.58	14.49 *	0.0125
AB	5.84	6.66	136.31	1	136.31	0.7692 ^{NS}	0.4206
AC	−0.7050	6.66	1.99	1	1.99	0.0112 ^{NS}	0.9198
BC	13.95	6.66	777.85	1	777.85	4.39 ^{NS}	0.0903
A^2	−3.34	6.93	41.10	1	41.10	0.2319 ^{NS}	0.6504
B^2	−15.63	6.93	902.16	1	902.16	5.09 ^{NS}	0.0737
C^2	−4.44	6.93	72.91	1	72.91	0.4115 ^{NS}	0.5495
Residual			886.03	5	177.21		
Lack of Fit			596.37	3	198.79	1.37 ^{NS}	0.4478
Total			13,326.91	14			
conveying rate [d]							
Model			27.10	9	3.01	7.80 *	0.0179
A	0.5656	0.2196	2.56	1	2.56	6.63 *	0.0497
B	1.36	0.2196	14.87	1	14.87	38.54 **	0.0016
C	0.8360	0.2196	5.59	1	5.59	14.49 *	0.0125
AB	−0.2725	0.3106	0.2970	1	0.2970	0.7698 ^{NS}	0.4206
AC	0.0329	0.3106	0.0043	1	0.0043	0.0112 ^{NS}	0.9198
BC	−0.6509	0.3106	1.69	1	1.69	4.39 ^{NS}	0.0903
A^2	0.1557	0.3232	0.0895	1	0.0895	0.2319 ^{NS}	0.6504
B^2	0.7294	0.3232	1.96	1	1.96	5.09 ^{NS}	0.0737
C^2	0.2073	0.3232	0.1587	1	0.1587	0.4115 ^{NS}	0.5495
Residual			1.93	5	0.3858		
Lack of Fit			1.30	3	0.4327	1.37 ^{NS}	0.4478
Total			29.02	14			
Autumn blockage rate [e]							
Model			14,267.54	9	1585.28	12.98 **	0.0057
A	−15.14	3.91	1832.55	1	1832.55	15.01 *	0.0117
B	−22.98	3.91	4225.56	1	4225.56	34.60 **	0.0020
C	−18.47	3.91	2729.87	1	2729.87	22.36 **	0.0052
AB	10.57	5.53	447.11	1	447.11	3.66 ^{NS}	0.1139

Table 8. *Cont.*

Source	Coefficients	Standard Error	Sum of Squares	DF	Mean Square	F-Value	*p*-Value
AC	−10.12	5.53	409.86	1	409.86	3.36 ^{NS}	0.1264
BC	19.36	5.53	1498.85	1	1498.85	12.27 *	0.0172
A^2	12.34	5.75	561.98	1	561.98	4.60 ^{NS}	0.0848
B^2	−1.61	5.75	9.55	1	9.55	0.0782 ^{NS}	0.7910
C^2	26.84	5.75	2659.31	1	2659.31	21.78 **	0.0055
Residual			610.56	5	122.11		
Lack of Fit			358.74	3	119.58	0.9497 ^{NS}	0.5496
Total			14,878.1	14			
conveying rate [f]							
Model			31.07	9	3.45	12.98 **	0.0057
A	0.7063	0.1823	3.99	1	3.99	15.01 *	0.0117
B	1.07	0.1823	9.20	1	9.20	34.60 **	0.0020
C	0.8621	0.1823	5.95	1	5.95	22.36 **	0.0052
AB	−0.4933	0.2578	0.9736	1	0.9736	3.66 ^{NS}	0.1139
AC	0.4725	0.2578	0.8931	1	0.8931	3.36 ^{NS}	0.1264
BC	−0.9033	0.2578	3.26	1	3.26	12.27 *	0.0172
A^2	−0.5757	0.2684	1.22	1	1.22	4.60 ^{NS}	0.0848
B^2	0.0751	0.2684	0.0208	1	0.0208	0.0783 ^{NS}	0.7910
C^2	−1.25	0.2684	5.79	1	5.79	21.78 **	0.0055
Residual			1.33	5	0.2659		
Lack of Fit			0.7812	3	0.2604	0.9497 ^{NS}	0.5496
Total			32.4	14			

Note: A, fan outlet wind speed; B, pipe inlet angle; C, feed-inlet side length. * $p < 0.05$, ** $p < 0.01$, NS—Not Significant. [a]: Spring blockage rate model: $R^2 = 0.9260$, adjusted $R^2 = 0.7929$, and predicted $R^2 = 0.3798$. [b]: Spring conveying rate model: $R^2 = 0.9260$, adjusted $R^2 = 0.7929$, and predicted $R^2 = 0.3798$. [c]: Summer blockage rate model: $R^2 = 0.9335$, adjusted $R^2 = 0.8138$, and predicted R^2 was 0.2351. [d]: Summer conveying rate model: $R^2 = 0.9335$, adjusted $R^2 = 0.8138$, and predicted R^2 was 0.2351. [e]: Autumn blockage rate model: $R^2 = 0.9590$, adjusted $R^2 = 0.8851$, and predicted R^2 was 0.5761. [f]: Autumn conveying rate model: $R^2 = 0.9590$, adjusted $R^2 = 0.8851$, and predicted R^2 was 0.5761.

The fitted regression equations for blockage rate and conveying rate of spring, summer, and autumn leaves are given in Equations (17)–(22).

$$Y = 10.93 - 13.78 \times A - 25.62 \times B + 19.76 \times C + 10.27 \times AB + 8.18 \times AC - 16.13 \times BC + 16.57 \times A^2 - 1.45 \times B^2 + 25.29 \times C^2 \quad (17)$$

$$Y = 4.16 + 0.6429 \times A + 1.2 \times B - 0.9221 \times C - 0.4792 \times AB - 0.3817 \times AC + 0.7525 \times BC - 0.7734 \times A^2 + 0.0674 \times B^2 - 1.18 \times C^2 \quad (18)$$

$$Y = 50.7 - 12.12 \times A - 29.21 \times B + 17.92 \times C + 5.84 \times AB + 0.705 \times AC - 13.95 \times BC - 3.34 \times A^2 - 15.63 \times B^2 - 4.44 \times C^2 \quad (19)$$

$$Y = 2.3 + 0.5656 \times A + 1.36 \times B - 0.836 \times C - 0.2725 \times AB - 0.0329 \times AC + 0.6509 \times BC + 0.1557 \times A^2 + 0.7294 \times B^2 + 0.2073 \times C^2 \quad (20)$$

$$Y = 8.34 - 15.14 \times A - 22.98 \times B + 18.47 \times C + 10.57 \times AB + 10.12 \times AC - 19.36 \times BC + 12.34 \times A^2 - 1.61 \times B^2 + 26.84 \times C^2 \quad (21)$$

$$Y = 4.28 + 0.7063 \times A + 1.07 \times B - 0.8621 \times C - 0.4933 \times AB - 0.4725 \times AC + 0.9033 \times BC - 0.5757 \times A^2 + 0.0751 \times B^2 - 1.25 \times C^2 \quad (22)$$

where Y is the predicted response; A, fan outlet wind speed; B, pipe inlet angle; and C, feed-inlet side length.

As shown in Table 8, the regression models for the pipe blockage rate and conveying rate of fresh tea leaves in all three seasons were significant ($p < 0.05$), and their lack-of-fit

terms were not significant. The R^2 values of the models ranged from 0.9260 to 0.9590, and the adjusted R^2 values ranged from 0.7929 to 0.8851, indicating good overall in-sample fit to the simulation data. However, the predicted R^2 values were only 0.2351–0.5761, substantially lower than the corresponding R^2 values, indicating limited capability to predict new observations. Therefore, these models should be interpreted as approximate descriptions of average response trends within the design space and used for comparing factor effects and screening engineering parameters, rather than for precisely predicting the outcomes of individual experimental runs. The model conclusions are limited to fan outlet air velocities of 20–30 m/s, pipe inlet angles of 10–20°, and feed inlet side lengths of 0.120–0.150 m. The actual conveying performance under the optimized operating conditions requires further experimental evaluation. The significant terms and fitting performance differed among the seasonal models. The autumn model showed the best fit ($F = 12.98$, $R^2 = 0.9590$), with significant linear, interaction, and quadratic terms, indicating pronounced interaction effects among the factors. The summer model showed the next-best fit, with significant terms dominated by linear effects, whereas the spring model had the relatively lowest fit and exhibited more pronounced nonlinear characteristics. Pipe inlet angle and feed inlet side length were significant in the models for all three seasons and were therefore identified as common key parameters affecting conveying performance. To assess the statistical assumptions of the regression model, the residuals of the autumn model were examined for normality, independence, and homoscedasticity. The residual analysis results are shown in Figure 7.

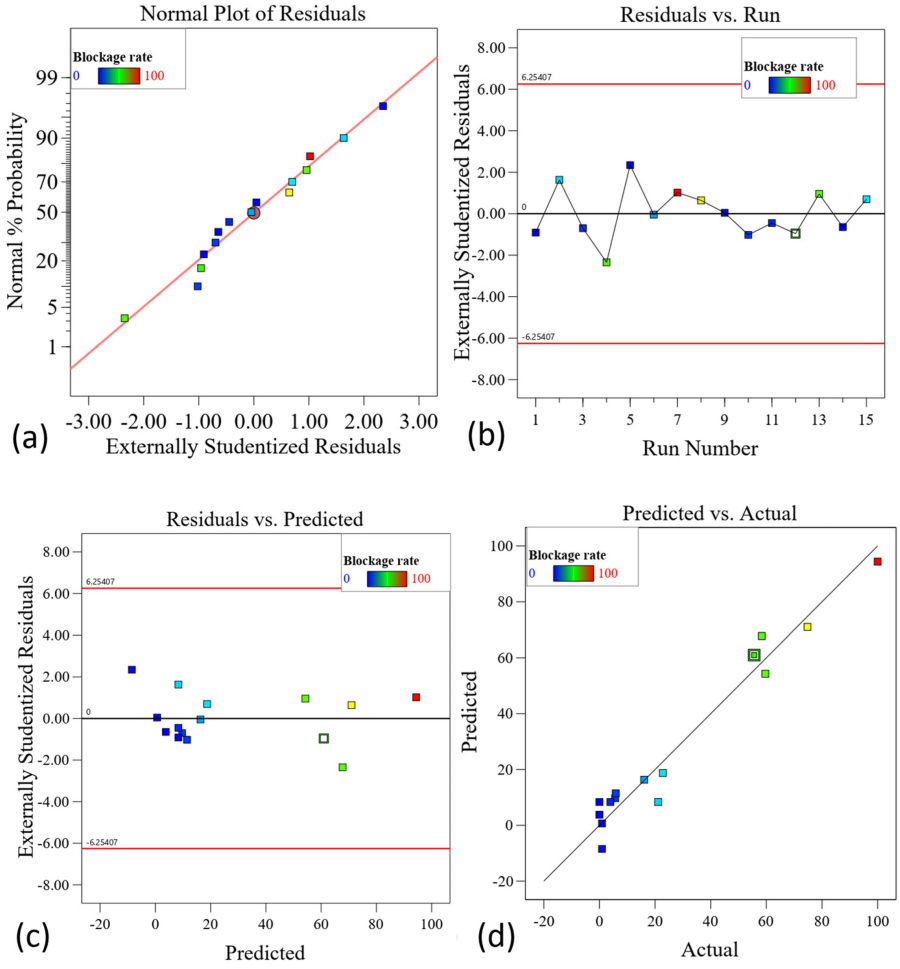


Figure 7. Residual diagnostic plots for the autumn blockage-rate model. (**a**) Externally studentized residuals; (**b**) Run number; (**c**) Predicted; (**d**) Actual.

As shown in Figure 7, the externally studentized residuals fell approximately along the theoretical straight line, indicating approximate normality (Figure 7a); the residuals fluctuated randomly on both sides of zero with run order and stayed within the control limits, showing no systematic deviation (Figure 7b); they were evenly distributed over the entire range of predicted values with no funnel-shaped heteroscedasticity (Figure 7c); and the predicted values agreed well with the actual values along the diagonal (Figure 7d). Overall, the regression model satisfies the underlying statistical assumptions, no obvious systematic pattern was observed in the residuals, and the predictions are of engineering reference value.

3.2.2. Effects of Pneumatic Conveying Pipeline Parameters on the Blockage Rate

The blockage rate is the core negative evaluation indicator. With the feeding-inlet side length fixed, the interactive effects of the fan outlet air velocity and the pipe inlet angle on the blockage rate of tea leaves in the three seasons are shown in Figure 8. The overall patterns can be summarized in three aspects:

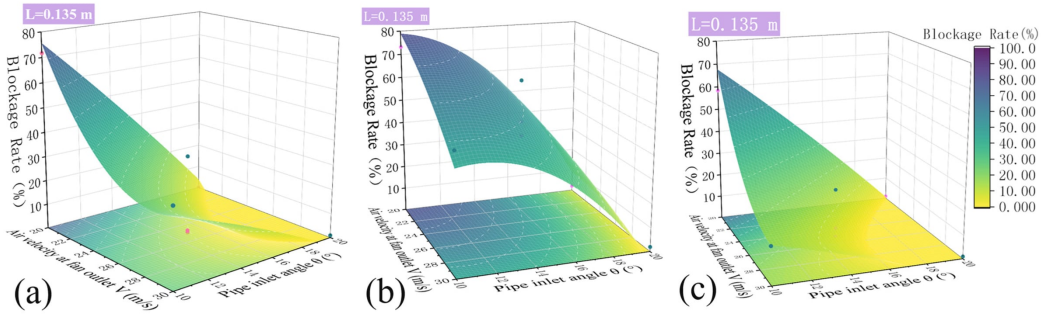


Figure 8. Response surface plots of the effects of fan outlet air velocity and pipe inlet angle on the blockage rate: (**a**) spring tea; (**b**) summer tea; (**c**) autumn tea, with feeding-inlet side lengths of 0.135 m.

For summer and autumn fresh tea leaves, the predicted average blockage rate consistently decreased with increasing fan outlet air velocity and pipe inlet angle. For all three seasons, the feed inlet side length exhibited a nonlinear effect on the blockage rate, characterized by an initial decrease followed by an increase, with a model-estimated optimal range of 0.135–0.146 m. The interaction between pipe inlet angle and feed-inlet side length was significant for autumn leaves: the smaller the side length, the more pronounced the blockage reduction achieved by increasing the inlet angle.

Taking the autumn leaves as an example, the parameter effects can be quantified as follows: At a feed-inlet side length of 0.135 m and an inlet angle of 10°, raising the wind speed from 20 to 30 m/s reduced the blockage rate from 67.76% to 16.35%, a relative reduction of 75.9%. At 25 m/s and the same side length, increasing the inlet angle from 10° to 20° reduced the blockage rate from 31.02% to 4.86%, a relative reduction of 84.3%. The spring-leaf case illustrates the nonlinear effect of the side length: at 25 m/s and 15°, increasing the side length from 0.12 to 0.135 m reduced the blockage rate from 78.14% to 10.93%, whereas a further increase to 0.15 m raised it back to 37.83%, indicating that an inlet size either too small or too large is unfavourable for blockage reduction.

The interaction effect is also evident. For autumn leaves at a side length of 0.12 m, increasing the inlet angle from 10° to 20° lowered the blockage rate by about 88.6%, while at 0.15 m the same angular adjustment produced only about 33.2% reduction. This pattern is useful in engineering design: the side length should be locked within the optimal range in the first place; where structural constraints force a smaller inlet, the conveying performance can be compensated by increasing the pipe inlet angle, whereas a larger inlet calls for a

higher wind speed as the main compensating measure. In any case, the inlet size should be kept from exceeding the optimal range at the design stage.

3.2.3. Effects of Pneumatic Conveying Pipeline Parameters on the Conveying Rate

The conveying rate, a positive index of operating efficiency, is shown in Figures 9 and 10. Figure 9 gives the response surfaces of conveying rate for summer leaves with respect to fan outlet wind speed and feed-inlet side length at different pipe inlet angles, and Figure 10 gives the corresponding surfaces for autumn leaves with respect to wind speed and inlet angle at different side lengths.

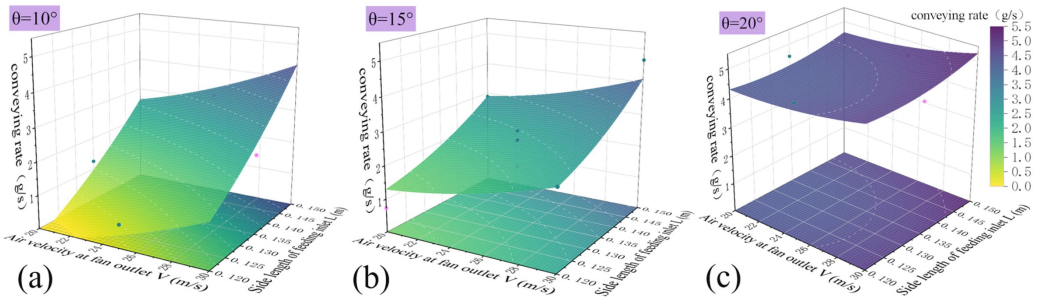


Figure 9. Response surface plots of the effects of fan outlet air velocity and feeding-inlet side length on the conveying rate of summer tea at different pipe inlet angles: (**a**) $\theta = 10°$; (**b**) $\theta = 15°$; (**c**) $\theta = 20°$.

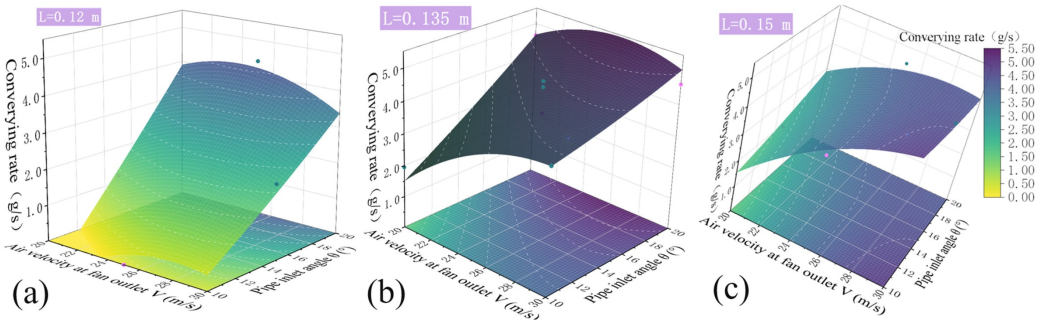


Figure 10. Response surface plots of the effects of fan outlet air velocity and pipe inlet angle on the conveying rate of autumn tea at different feeding-inlet side lengths: (**a**) $L = 0.12$ m; (**b**) $L = 0.135$ m; (**c**) $L = 0.15$ m.

Overall, the pipe inlet angle had a marked main effect: at identical operating conditions, the conveying rate increased with the angle, ranking 20° > 15° > 10°. At a fixed angle, raising the wind speed or tuning the side length both improved the conveying rate. The side length itself showed a quadratic, non-monotonic effect—the rate first rose and then fell with increasing side length, peaking near 0.135 m, with the overall ranking being 0.135 m > 0.15 m > 0.12 m.

When the side length was small, the feeding cross-section was restricted and fresh leaves tended to jam at the inlet; under such conditions, raising the wind speed or enlarging the angle gave only limited improvement in the conveying rate, and the overall operating efficiency stayed low. With the side length in the optimal range of 0.135 m, the conveying rate increased markedly over the whole operating window, giving the widest range of high-efficiency conditions. When the side length was further increased to 0.15 m, the local airflow at the inlet weakened and the gain in conveying rate levelled off, showing diminishing marginal returns.

For engineering selection, a feed-inlet side length of 0.135 m accommodates both a low blockage rate and a high conveying rate, making it the structural parameter with the best overall performance.

3.3. Optimization of Pneumatic Conveying Pipeline Parameters

To obtain the optimal operating conditions, the blockage rate was minimized by the desirability function method, with the conveying rate incorporated as a derived engineering index; the two responses were weighted equally at 50% each. Before optimization, the response indicators were dimensionless-normalized by range standardization: minimization standardization was applied to the blockage rate and maximization standardization to the fresh-leaf conveying rate, and the two were then weighted to calculate a composite score (out of 1.0, with a higher score indicating better overall performance of the system). Fan outlet air velocity (20–30 m/s), pipe inlet angle (10–20°), and feed inlet side length (0.120–0.150 m) were used as optimization variables. Random searches of 250 points within the experimental factor ranges were conducted, and the response surface models for spring, summer, and autumn tea leaves were optimized independently to obtain season-specific operating-parameter combinations. The optimal parameters were substituted into the corresponding quadratic regression models to calculate the predicted responses. When a negative blockage rate was predicted, it was regarded as a non-physical mathematical prediction of the empirical model. The blockage rate was therefore constrained to nonnegative values, with zero as the lower bound. This treatment was used only for parameter screening and should not be interpreted as evidence that zero blockage would necessarily occur under actual operating conditions. Multiple solutions with an overall desirability of 1.0 indicated a broad optimal plateau rather than a single unique optimum. The final parameters were therefore selected within the design space according to engineering criteria. Based on engineering practicality, a common structural configuration was selected: the pipe inlet angle was fixed at 20°, the feed inlet side length was fixed at 0.135 m, and only the fan outlet air velocity was retained as an adjustable parameter. The air velocity could be adjusted within the range of 25–30 m/s according to seasonal variations in the physical properties of fresh tea leaves, with 30 m/s recommended for spring and summer tea leaves and 25 m/s for autumn tea leaves. This configuration requires only one pipe structure and allows seasonal adaptation through fan speed adjustment, thereby providing a practical compromise between predicted conveying performance and engineering cost considerations. The results are shown in Table 9.

Table 9. Desirability-function-based optimal parameter combinations and predicted performance for the three seasons of tea leaves.

Season	Air Velocity/ ($m \cdot s^{-1}$)	Inlet Angle/ (°)	Side Length/ (m)	Predicted Blockage Rate/ (%)	Predicted Conveying Rate/ ($g \cdot s^{-1}$)	Desirability Score
Spring	29.07	17.94	0.135	0	4.667	1
Summer	29.69	19.61	0.138	0	4.667	1
Autumn	25.02	19.80	0.146	0	4.667	1

3.4. Field Experiment Feasibility

To verify the applicability of a single structural unit to the fresh leaves of all three seasons, field harvesting experiments of bulk tea were conducted at the Huangma Tea Base in Nanchang County and the Tea Mechanization Research Base in Gao'an City, Jiangxi Province, on 10–12 May 2026 (spring), 8–10 July 2026 (summer), and 28–30 August 2026 (autumn), respectively. The tea cultivars at the two bases are Fuding Dabai and a local cultivar, respectively; the tea trees at both bases are over 40 years old, with stable growth

and regular canopies, meeting the conditions for mechanized harvesting. Specifically, at the Huangma Base, the canopy height is about 80 cm, the canopy width about 100 cm, and the row spacing about 150 cm; at the Gao'an Base, the corresponding values are about 100 cm, 100 cm, and 140 cm.

In each experimental tea garden, plots with uniform growth and no pests or diseases were randomly selected, and a standard working area of 20 m in length was marked out. Before the experiments, the harvester header was adjusted to an appropriate position, and the fan outlet air velocity was set to 30 m/s(autumn leaves were tested at the upper fan limit of 30 m/s, while 25 m/s represents the energy-saving condition recommended by the model). The cutter, conveying auger, fan, and other working motors were started in sequence, and harvesting began after the motor speeds and pipeline airflow reached a stable operating state. If pipeline blockage occurred during operation, the accumulated fresh leaves in the pipe were promptly removed before harvesting was resumed. To reduce field random errors and ensure data reliability, the harvesting operation was repeated 10 times under each experimental condition, and the average blockage rate was calculated. The calculation of the blockage rate was consistent with the simulation evaluation indicator, as given in Equation (14). The field experiment sites for the three seasons are shown in Figure 11.



Figure 11. Field experiment sites: (**a**) spring experiment (10 May 2026); (**b**) summer experiment (8 July 2026); (**c**) autumn experiment (28 August 2026).

The experimental results are presented in Table 10.

Table 10. Results of the field experiments.

Site	Outlet Mass/kg	Spring Retained Mass/kg	Blockage Rate/%	Outlet Mass/kg	Summer Retained Mass/kg	Blockage Rate/%	Outlet Mass/kg	Autumn Retained Mass/kg	Blockage Rate/%
Huangma Base, Nanchang	5.63	0.00	0.00	5.35	0.00	0.00	4.83	0.00	0.00
	5.71	0.00	0.00	5.50	0.00	0.00	4.95	0.00	0.00
	5.87	0.00	0.00	5.29	0.00	0.00	4.89	0.00	0.00
	6.49	0.00	0.00	5.18	0.00	0.00	4.51	0.00	0.00
	6.41	0.00	0.00	4.99	0.00	0.00	4.91	0.00	0.00
	6.79	0.00	0.00	5.46	0.28	4.88	4.65	0.00	0.00
	6.25	0.00	0.00	5.43	0.31	5.40	4.79	0.00	0.00
	6.13	0.00	0.00	5.23	0.00	0.00	5.12	0.00	0.00
	6.46	0.00	0.00	5.16	0.00	0.00	4.73	0.00	0.00
	6.40	0.00	0.00	5.32	0.00	0.00	4.46	0.00	0.00
Gao'an Base, Yichun	5.21	0.00	0.00	4.02	0.00	0.00	3.53	0.00	0.00
	5.40	0.00	0.00	4.11	0.00	0.00	3.17	0.00	0.00
	5.36	0.00	0.00	3.96	0.00	0.00	3.76	0.00	0.00
	5.79	0.00	0.00	4.79	0.00	0.00	2.98	0.00	0.00
	6.14	0.00	0.00	3.98	0.00	0.00	3.46	0.00	0.00
	6.23	0.00	0.00	3.94	0.00	0.00	3.89	0.00	0.00
	5.79	0.00	0.00	4.88	0.00	0.00	3.16	0.00	0.00
	5.61	0.00	0.00	4.13	0.00	0.00	3.34	0.00	0.00
	5.59	0.00	0.00	4.16	0.00	0.00	3.54	0.00	0.00
	6.28	0.00	0.00	4.86	0.00	0.00	3.42	0.00	0.00

The field experiment results (Table 10) show that, under the optimized parameter combination of a fan outlet air velocity of 30 m/s, a pipe inlet angle of 20°, and a feeding-inlet side length of 0.135 m, the pneumatic conveying device achieved stable conveying of bulk fresh tea leaves in all three seasons. Specifically, in the spring experiment, the total mass of tea leaves discharged at the outlet was 119.54 kg, with no accumulation in the pipeline and a blockage rate of 0.00%; in autumn, the total outlet mass was 82.09 kg, again with no accumulation and a blockage rate of 0.00%; and in summer, the total outlet mass was 95.74 kg, with 0.59 kg retained in the pipeline, giving a blockage rate of 0.61%. The summer blockage was caused by an incidental condition: the ground of part of the experimental tea ridge was uneven, the header sank passively during operation, and old stems at the bottom of the canopy were harvested. A plausible explanation is that these old stems are long and heavy, and their physical properties differ significantly from those of normally harvested fresh leaves; they tend to become jammed in the conveying pipeline and gradually entangle and aggregate into flocs, thereby inducing local blockage. The morphology of the blocked fresh leaves and old stems is indicated by the red circle in Figure 12.



Figure 12. Blocked fresh tea leaves and old stems in the pipeline (indicated by the red circle).

4. Discussion

This study addressed the optimal design of pneumatic conveying pipes for bulk fresh tea leaves from three aspects: the realism of particle modelling, the matching of structural parameters, and the adaptability to seasonal material properties. The non-spherical flake-particle model reveals the aerodynamic essence that distinguishes fresh leaves from near-spherical materials, which essentially sets the direction for structural parameter optimization; in turn, the optimal combination of structural parameters is constrained by seasonal variations in physical properties and directly affects the year-round applicability of field equipment. The following discussion interprets the mechanistic implications and practical significance of the findings from these three perspectives.

Regarding particle modelling, the fidelity of the geometric model strongly affects pneumatic conveying simulations. Most previous studies on agricultural materials approximate the particles as spherical or near-spherical, which cannot reproduce the true flow-following behaviour of thin, flake-like tea leaves in an airstream. Although Weng [15] constructed a particle model of machine-harvested fresh leaves by multi-sphere clustering, the actual leaf outline was not reconstructed. In this study, one-leaf, two-leaf, and three-leaf geometries were reconstructed from 3D scans, and ball-cluster non-spherical flake particles were generated through multi-sphere filling, reproducing the large aspect ratio and irregular outline of real leaves; this is the prerequisite for the model to reproduce floc formation and wall-adhering migration. The improvement at the modelling level has a fundamental bearing on the subsequent optimization: because the drag-facing resistance of a non-spherical particle is markedly higher than that of an equal-volume near-spherical particle, a higher wind speed is required to maintain stable suspension conveying—this explains why fan outlet wind speed was significant in both the summer and autumn regression models.

As for the structural parameters of the conveying device, coupling and nonlinear effects were evident. The feed-inlet side length showed a marked nonlinear effect on conveying performance, with an optimal range of 0.135–0.146 m, which is consistent with the finding of Du [12] that the main-pipe taper, branch number, and branch outlet diameter of a leaf-collecting pipeline all affect the mean outlet air velocity and its uniformity in a non-monotonic manner. Compared with near-spherical materials, however, thin flake leaves are more sensitive to the inlet size, essentially because of their large spatial occupation and tendency to overlap. A side length that is too small makes particles squeeze and overlap into flocs, whereas one that is too large weakens the air-carrying capacity. Such a nonlinear effect is not pronounced for near-spherical materials, highlighting the need for structure-oriented optimization specific to flake leaves. The pipe inlet angle acts mainly through the jet direction, which shapes the in-pipe pressure gradient and flow-field distribution; this mechanism agrees with studies on how inlet structural parameters affect the performance of pneumatic seed-metering devices [33]. The optimal wind-speed range identified in this study (25–30 m/s) is close to the best leaf-collecting velocity (about 25 m/s) obtained by Weng [15] through single-factor simulation, although that study considered only a single leaf population and bend configuration, without seasonal differences or parameter interactions. Du [12] and Weng [11], whose work dealt with pure airflow fields, evaluated outlet uniformity rather than particle conveying performance. The interaction between side length and inlet angle further supports this prioritization: at a small side length, the blockage reduction achieved by adjusting the angle (88.6%) was about 2.67 times that at a large side length (33.2%); the side length should therefore be locked in first during design and strictly kept within the optimal range. The estimated field feeding rates were approximately 15–21 times the reference value used in the simulations, corresponding to solids-to-air mass ratios of approximately 0.60–0.88 and nominal particle volume fractions of approximately 0.13–0.21%. Based on the cross-sectionally averaged particle volume fractions, the overall field conveying process remained characteristic of dilute-phase transport. Therefore, one-way coupling may serve as an engineering approximation during stable conveying when the particles are well dispersed. However, the solid-to-air loading under field conditions was substantially higher than that under the simulation conditions, and the above volume-fraction estimates did not account for particle slip, prolonged residence times, or local particle accumulation at the feed inlet and within the pipe bends. At high feeding rates and during blockage formation, the effects of the particle phase on the gas-phase flow field may not be negligible. Therefore, the applicability of the current one-way coupling model at actual field feeding rates has not been fully validated, and the model predictions obtained at 7 g/s are not directly extrapolated quantitatively to field conditions. Further

evaluation is required through comparisons between particle-free and particle-laden flow fields, feeding-rate sensitivity analyses, and two-way coupled simulations.

As for material differences, the physical properties of fresh tea leaves constrain the conveying parameters across seasons. The seasonal differences in conveying behaviour originate essentially from changes in physical properties, yet almost all previous studies tested leaves with a single set of properties. In this study, the physical properties of the three seasonal crops were sampled in 2025, and field validation was conducted in 2026 at two tea bases (Nanchang County and Gao'an City) from 10 to 12 May (spring), 8 to 10 July (summer), and 28 to 30 August (autumn). The device conveyed all three seasonal crops stably, with measured blockage rates of 0.00% in spring and autumn and 0.61% in summer, confirming the practical applicability of the unified scheme. One possible explanation for the higher predicted blockage rates of spring leaves under some conditions is moisture-associated adhesion and agglomeration. Similarly, the seasonal differences in conveying behavior may be related to variations in leaf density, fibrous structure, stiffness, and moisture content. However, interparticle adhesion and single-leaf suspension velocity were not directly measured, and the respective contributions of these properties were not isolated in this study. Therefore, these mechanisms are proposed only as possible explanations and require further experimental verification. These seasonal property–performance relationships enrich the property-adaptation theory for pneumatic conveying of flake-like agricultural products. Industrial pneumatic conveying studies on lightweight, irregularly shaped materials, such as cut tobacco [34], have shown that low-density components respond rapidly to airflow and exhibit short residence times, whereas high-density rigid components are more likely to remain near the pipe wall at bends. In the present study, the relatively high blockage rate for spring tea leaves may have been dominated by adhesion and agglomeration associated with high moisture content and may therefore not be adequately explained by the density–rigidity framework. This suggests that conveying behavior established for dry, homogeneous materials cannot be directly extrapolated to fresh tea leaves with high moisture content. The measured blockage rate of 0.61% for summer tea leaves may have resulted from the intake of old stems when the cutting header was lowered, also suggesting that the robustness of the selected parameter combination may be limited when material properties deviate from the ranges considered during model development. However, interparticle adhesion was not directly measured in this study, and neither dynamic adhesion nor leaf deformation was represented in the DEM model. Therefore, the aforementioned mechanisms are proposed only as possible explanations and require further verification through dedicated experiments.

Several methodological limitations should be considered when interpreting the conclusions. First, the DEM model adopted fixed, mean-value physical parameters, whereas real leaves vary individually in shape and mechanical properties, which introduces uncertainty into the simulation results; future work could adopt parameter schemes accounting for such distributions to improve the prediction of particle motion. Second, although the ball-cluster model reproduced the macroscopic leaf outline, the rigid-particle assumption neglects leaf micro-deformation and dynamic adhesion, which may lead to an underestimation of floc formation under the high-moisture spring condition; deformable leaf particles could be developed in future work by reference to immersed-boundary–lattice-Boltzmann coupling methods, so as to fully resolve micro-deformation and dynamic adhesion. Third, the response-surface design space was built on three factors at three levels and did not cover field disturbances such as tea cultivar, pipe-wall roughness, or ambient temperature and humidity; the field robustness of the optimized parameters therefore awaits verification with larger samples over longer periods.

5. Conclusions

By combining CFD–DEM coupled simulation, Box–Behnken response surface experiments, and field feasibility evaluation at two sites across three seasons, this study established a complete research pathway of "mechanism revelation–parameter optimization–engineering feasibility evaluation" for the pneumatic conveying device with bend pipes in self-propelled tea harvesters for hilly areas. The main advances are as follows:

CFD–DEM simulations showed that the low-velocity triangular recirculation zone near the lower wall of the pipe inlet and the low-velocity zone on the inner side of the pipe bends were the main locations associated with a risk of fresh tea leaf deposition. Increasing the pipe inlet angle reduced the low-velocity recirculation zone at the inlet and improved the initial acceleration conditions of the leaves. Velocity stratification, characterized by higher velocities on the outer side and lower velocities on the inner side of the bends, together with transverse pressure differences and recirculation vortices, occurred concomitantly with particle–wall contact and localized particle retention. The airflow across the outlet cross-section was generally relatively uniform, with no distinct low-velocity stagnation zones. The effect of air velocity on conveying stability was non-monotonic. A moderate increase in air velocity enhanced particle suspension and transport, whereas excessive air velocity could intensify flow disturbances and local vortices in the bends, thereby compromising conveying stability.

The quadratic regression models for the blockage rate and conveying rate of fresh tea leaves in all three seasons were significant ($p < 0.05$), and their lack-of-fit terms were not significant. The R^2 values of the spring, summer, and autumn models were 0.9260, 0.9335, and 0.9590, respectively, and the adjusted R^2 values of the models ranged from 0.7929 to 0.8851, indicating good overall in-sample fit to the available simulation data. However, the predicted R^2 values were only 0.2351–0.5761, substantially lower than the corresponding R^2 values, indicating limited capability to predict new observations. Therefore, these models were primarily used to describe conditional average trends in blockage rate and conveying rate as functions of the investigated factors within the experimental design space and to provide a reference for comparing factor effects and screening parameters, rather than to precisely predict the results of individual simulations or field trials. Pipe inlet angle and feed inlet side length were common significant factors in the models for all three seasons. According to the significance analysis, the factors affecting conveying performance were ranked as pipe inlet angle > feed inlet side length > fan outlet air velocity for both summer and autumn tea leaves, whereas conveying performance for spring tea leaves was mainly affected by pipe inlet angle and feed inlet side length. Overall, the model trends suggested season-dependent benefits of increasing pipe inlet angle for reducing blockage and improving conveying rate, with diminishing improvement under some high-air-velocity conditions. The feed inlet side length exhibited nonlinear effects: the blockage rate first decreased and then increased with increasing side length, whereas the conveying rate first increased and then decreased.

The factor-interaction analysis further showed that the feed inlet side length modified the effect of the pipe inlet angle. According to estimates from the autumn model, when the feed inlet side length was 0.120 m, increasing the pipe inlet angle from 10° to 20° corresponded to a predicted reduction in blockage rate of approximately 88.6%. At a side length of 0.150 m, the same angular adjustment corresponded to a predicted reduction of approximately 33.2%. These values were model estimates intended to illustrate the direction and relative strength of the interaction, rather than measured reductions from independent experiments. The model trends also indicated that the relatively favorable feed inlet side length ranges for reducing blockage were approximately 0.135–0.146 m across the three seasons, whereas the favorable values for conveying rate were concentrated around 0.135 m.

This suggests that the feed inlet dimensions should not be determined solely according to the principle of increasing the flow cross-sectional area. Instead, they should be selected in conjunction with the pipe inlet angle to balance a lower blockage risk against a higher conveying rate.

Desirability-function analysis based on the above regression models identified parameter plateaus with an overall desirability score of 1.0 for all three seasons, rather than a unique mathematical optimum. This score reflects the model-based evaluation under the specified optimization objectives and weights and does not indicate that actual conveying performance would necessarily be optimal. Independent optimization of the seasonal models yielded pipe inlet angles of 17.94°, 19.61°, and 19.80°, and feed inlet side lengths of 0.135, 0.138, and 0.146 m for spring, summer, and autumn, respectively. Considering the overlap among the high-desirability parameter plateaus for the three seasons and the prototype manufacturing requirements, a common structural configuration was selected, comprising a pipe inlet angle of 20°and a feed inlet side length of 0.135 m. The model-based recommended adjustment range for fan outlet air velocity was 25–30 m/s, with 30 m/s recommended for spring and summer tea leaves and 25 m/s for autumn tea leaves. This common configuration represents an engineering choice that balances seasonal conveying requirements against the use of a common pipe structure. It does not replace the season-specific optimization results, and its actual performance requires further field evaluation.

Author Contributions: Conceptualization, L.W. and J.X.; Methodology, L.W. and J.X.; Software, J.X., C.D. and H.F.; Validation, L.W., J.X., S.S. and H.F.; Formal analysis, S.S. and C.D.; Investigation, J.X. and H.F.; Resources, H.F.; Data curation, J.X. and C.D. Writing—original draft, L.W. and J.X.; Writing—review & editing, L.W. and S.S.; Visualization, J.X., C.D. and H.F. Project administration, L.W.; Funding acquisition, L.W. and S.S. All authors have read and agreed to the published version of the manuscript.

Funding: This research was funded by the Department of Agriculture and Rural Affairs of Jiangxi Province under the Jiangxi Province Integrated Pilot Project for the Research, Development, Manufacturing, and Promotion and Application of Agricultural Machinery and Equipment (grant number YCTY22408), and by the Jiangxi Academy of Agricultural Sciences under the Jiangxi Modern Agricultural Research Collaborative Innovation Project (grant number JXXTCX202603).

Institutional Review Board Statement: Not applicable.

Informed Consent Statement: Not applicable.

Data Availability Statement: The original contributions presented in the study are included in the article; further inquiries can be directed to the corresponding author.

Conflicts of Interest: Author Fu Hao is affiliated with Jiangxi Shanyi Intelligent Equipment Co., Ltd., which manufactured the self-propelled bulk tea harvester evaluated in this study. The company did not provide research funding and had no role in data analysis, interpretation of the results, manuscript preparation, or the decision to publish.

References

1. International Tea Committee. 2025 Global Tea Statistical Bulletin. Available online: http://en.capiaccti.org.cn/marketandtrade/dde8ef4869cb9b62025b5c8f3bb51e5e (accessed on 7 November 2026).
2. Wu, C.; Wang, J.; Yang, Y.; Li, D.; Li, X.; Yan, R. Analysis of the development status and mechanization trends of economic crop industry in China. *J. Chin. Agric. Mech.* **2024**, *45*, 1–13. [CrossRef]
3. 2023 National Agricultural Mechanization Development Statistical Bulletin. Available online: https://njhs.moa.gov.cn/nyjxhqk/202511/t20251120_6479054.htm (accessed on 3 November 2026).
4. Liu, H.; Yao, Y.; Jiang, H.; Zhou, X.; Gan, N.; Lv, L.; Li, Z.; Zhang, L.; Dong, C.; Li, X.; et al. Research progress on picking/harvesting techniques, and equipment of tea shoots. *Beverage Plant Res.* **2026**, *6*, e027. [CrossRef]

5. Wang, W.; Xiao, H.; Song, Z.; Han, Y.; Ding, W. Research status and prospects of tea production mechanization technology. *J. Chin. Agric. Mech.* **2020**, *41*, 226–236. [CrossRef]
6. Luo, Z.-Y.; Chen, J.; Fang, J.-J.; Niu, P.; Zheng, Y.-L.; Wang, Y.-L.; Wang, L.; Zhang, M. Mechanization in Hilly and Mountainous Areas Current Situation and Development Suggestions of Tea Garden Planting. *J. Agric. Mech. Res.* **2020**, *42*, 1–7. [CrossRef]
7. Liu, H.; Xiao, Q.; Li, X.; Bai, J.; Wang, D.; Li, Y. Design and experiment of the stepped transportation tea harvesting and grading integrated machine. *Trans. Chin. Soc. Agric. Eng.* **2024**, *40*, 52–60. [CrossRef]
8. Jia, J.; Wang, D.; Zhao, X.; Wu, C.; Chen, J.; Yu, J. Design and Experiment of Picking and Collection Integrated End Effector for Famous Tea. *Trans. Chin. Soc. Agric. Mach.* **2026**, *57*, 274–284. [CrossRef]
9. Wu, L.; Liu, H.; Ye, C.; Wu, Y. Development of a Premium Tea-Picking Robot Incorporating Deep Learning and Computer Vision for Leaf Detection. *Appl. Sci.* **2024**, *14*, 5748. [CrossRef]
10. Huan, X.; Gao, X.; Wu, M.; Fan, G.; Wu, C.; Jia, J.; Chen, J. Design and Experiment of Key Devices for Self-propelled Bulk Tea Canopy Surface Shaping Tea Picking Machine. *Trans. Chin. Soc. Agric. Eng.* **2025**, *56*, 374–383. [CrossRef]
11. Weng, X.; Tan, D.; Wang, G.; Chen, C.; Zheng, L.; Yuan, M.; Li, D.; Chen, B.; Jiang, L.; Hu, X. CFD Simulation and Optimization of the Leaf Collecting Mechanism for the Riding-Type Tea Plucking Machine. *Agriculture* **2023**, *13*, 946. [CrossRef]
12. Du, Z.; Zhang, L.; Li, X.; Jin, X.; Yu, F. Optimizing Efficiency of Tea Harvester Leaf-Collection Pipeline: Numerical Simulation and Experimental Validation. *Agriculture* **2024**, *14*, 653. [CrossRef]
13. Liu, H.; He, F.; Li, R.; He, H.; Wang, Y. Design and Test of Portable Vacuum Absorption Tea Collector. *J. Agric. Mech. Res.* **2021**, *43*, 110–114. [CrossRef]
14. Chen, J.; Li, H.; Ren, P.; Jia, J.; Zhao, R.; Wu, C. Design and Experiment of Threaded Tube Adsorption Type Famous Tea Harvester. *Trans. Chin. Soc. Agric. Mach.* **2023**, *54*, 131–139. [CrossRef]
15. Weng, X.; Chen, C.; Wang, G.; Wei, Z.; Jiang, L.; Hu, X. Numerical Simulation of Leaf Gathering Process of Fresh Leaf Collecting Pipeline Based on CFD-DEM. *Trans. Chin. Soc. Agric. Mach.* **2022**, *53*, 424–432. [CrossRef]
16. Zhang, X.; Yang, T.; Qiao, X.; Zhong, J.; Ou, C.; Wang, S.; Zhou, Z. Study on Effect of Air Inlet Flow Field on the Tea Particles Drift Distance and Quality of Wind-selecting. *J. Tea Sci.* **2013**, *1*, 60–66.
17. Luo, K.; Cao, C.; Wu, Z.; Zhang, X.; An, M. Optimization of Roasted Green Tea Winnowing via Fluid–Solid Interaction Experiments and Simulations. *Foods* **2022**, *11*, 3271. [CrossRef] [PubMed]
18. Wang, R.; Wei, Y.; Wu, C.; Sun, L.; Zheng, W. Numerical simulation of motion characteristics of flexible fresh tea leaf in Poiseuille shear flow via combined immersed boundary–lattice Boltzmann method. *Int. J. Mod. Phys. C* **2019**, *30*, 1950038. [CrossRef]
19. Zhang, K.; Ma, G.; Hu, F.; Gao, H.; Zhang, C.; Zhang, X. Design of Equipment and Experiment on Air Separation Performance of Green Tea. *Trans. Chin. Soc. Agric. Mach.* **2023**, *54*, 366–374, 387.
20. Li, J.; Huang, Z.; Jiang, Y.; Cui, Z.; Zhang, M.; Zang, Y.; Qin, W. Design and test of a precision air-suction maize seed-metering device for plot planting based on CFD-DEM coupling. *Comput. Electron. Agric.* **2025**, *238*, 110888. [CrossRef]
21. Wang, P.; Wang, H.; Zhang, R.; Hu, R.; Hao, B.; Huang, J. Numerical Simulation of an Online Cotton Lint Sampling Device Using Coupled CFD–DEM Analysis. *Agriculture* **2024**, *14*, 127. [CrossRef]
22. He, B.; Zeng, H.; Ge, Y.; Li, G.; Ma, C.; Zheng, Y.; Guo, Y. Optimization of structural parameters for the pneumatic conveying device of dried safflower filaments based on CFD-DEM coupling. *Results Eng.* **2026**, *29*, 109092. [CrossRef]
23. Lin, Y.-P.; Jin, X.-Y.; Hao, Z.-L.; Ye, N.-X.; Huang, Y.-B.; Tang, H.-Y.; Chen, X.-H.; Zhou, X.-Y. Experiment on Mechanical Properties and Crude Fiber of Tea Leaf. *J. Tea Sci.* **2013**, *33*, 364–369. [CrossRef]
24. Du, Z.; Li, D.; Li, X.; Jin, X.; Wu, Y.; Yu, F. Calibration and Experiment of Discrete Element Model Parameters for Tea Stem. *Trans. Chin. Soc. Agric. Mach.* **2025**, *56*, 311–320. [CrossRef]
25. El-Emam, M.A.; Shi, W.; Zhou, L. CFD-DEM simulation and optimization of gas-cyclone performance with realistic macroscopic particulate matter. *Adv. Powder Technol.* **2019**, *30*, 2686–2702. [CrossRef]
26. Sun, L.; Jin, G.; Wang, Y.; Chen, J.; Yu, G. Discrete Element Model Construction and Parameter Calibration of Flexible Leaves in Rice Pot Seedlings. *Trans. Chin. Soc. Agric. Mach.* **2026**, *57*, 259–268. [CrossRef]
27. Krüger, T.; Varnik, F.; Raabe, D. Efficient and accurate simulations of deformable particles immersed in a fluid using a combined immersed boundary lattice Boltzmann finite element method. *Comput. Math. Appl.* **2011**, *61*, 3485–3505. [CrossRef]
28. Wang, Q.; Xu, Y. Simulation study on inertial focusing of curved flexible filaments based on IB-LBM. *Aip Adv.* **2026**, *16*, 55315. [CrossRef]
29. Li, J.; Su, N.; Wei, L.; Zhang, X.; Yin, Y.; Zhao, W. Study on the surface forming mechanism of the solid–liquid two-phase grinding fluid polishing pipe based on large eddy simulation. *Proc. Inst. Mech. Eng. Part B J. Eng. Manuf.* **2019**, *233*, 2505–2514. [CrossRef]
30. Ganser, G.H. A rational approach to drag prediction of spherical and nonspherical particles. *Powder Technol.* **1993**, *77*, 143–152. [CrossRef]
31. Zhang, C.; He, J.; Yang, S.; Qiao, Y.; Zhou, L.; Dai, L. Optimization of Airflow Field and Experimental Verification for Wheat Cleaning Device Based on CFD-DEM. *Fluids* **2026**, *11*, 85. [CrossRef]

32. Kang, Y.; Song, X.; Luo, R.; Huang, T.; Xiao, F.; Deng, Z.; Chen, H. CFD-DEM simulation and parameter optimization of pneumatic conveying of threshed corn residual products in a vertical elbow. *Ind. Crops Prod.* **2026**, *243*, 123012. [CrossRef]
33. Han, D.; Li, W.; Wang, Y.; Wang, Q.; Wu, Z.; Wang, Y.; Xu, Y.; Xu, L. CFD-DEM coupling analysis of the negative pressure inlet structural parameters on the performance of integrated positive-negative pressure seed-metering device. *Front. Plant Sci.* **2025**, *16*, 1485710. [CrossRef] [PubMed]
34. Tan, G.; Huang, D.; Wang, G.; Ding, D.; Wang, H.; Li, C.; Wang, Q.; Zhao, Y.; Wang, L.; Zhu, W. Numerical simulation study on the conveying characteristics of a multi-component flexible particle system in industrial pneumatic conveying pipeline. *Powder Technol.* **2025**, *466*, 121450. [CrossRef]

Disclaimer/Publisher's Note: The statements, opinions and data contained in all publications are solely those of the individual author(s) and contributor(s) and not of MDPI and/or the editor(s). MDPI and/or the editor(s) disclaim responsibility for any injury to people or property resulting from any ideas, methods, instructions or products referred to in the content.